Journal of Basrah Researches (Sciences) **52**(1), 204 (2026)
DOI: https://doi.org/10.56714/bjrs.52.1.15

A flexible graphene electrode for a high-performance flexible supercapacitor a large-area graphene-based electrode

Qassam R. Hasan*, Ahmed S. Al-Asadi

Department of Physics, College of Education for Pure Sciences, University of Basrah, Basrah, Iraq.

ARTICLE INFO

Received 23 February 2026
Revised 27 April 2026
Accepted 28 April 2026
Published 30 June 2026

Keywords:

Supercapacitor, Graphene, Roll-To-Roll, Flexibility.

Citation: Q. R. Hasan, A. S. Al-Asadi. , J. Basrah Res. (Sci.) **52**(1), 204 (2026). DOI:https://doi.org/10.56714/bjrs.52.1.15

ABSTRACT

In this report, graphene (G) layers were synthesized onto the top of Al substrate creating electrode for supercapacitor (SC). The obtained G@Al was used as flexible electrodes, and it shows a good stability with consist cycle voltammetry alone with good energy and power densities. The Highest Specific capacitance at flat conditions is about 17.629 Fg^{-1} and this value not dropped down more than 9.4% after bending the device with angle 30, 60, 90, 120, 150, and 180. The G@Al showed a good stability and it returns 93.5% from initial one after 1000 cycles. The maximum ED and PD were found to be as high as 5.5Wh/kg and.5.73kW/kg respectively, The EIS showed a good electrochemical performance and the ebullient circuit showed four resistance and CPE along with W element. Advancing the obtained SC by creating large area graphene based flexible supercapacitor device which showed a higher specific capacitance of 123.774 Fg^{-1} along with outstanding flexibility.

1. Introduction

In an effort to decrease pollution and carbon emissions[1-3] and increase the reliability of renewable energy sources like solar and wind[4, 5], researchers are focusing on the development of highly flexible energy storage systems[6-8]. These systems should be lightweight, thin, tiny[9], flexible, and capable of rolling up[10-12] . Among many energy storage systems, supercapacitors are the most promising candidates for flexible devices due to their advantages of high-power density[13], fast charge and discharge performance[13], and excellent cycling stability[14-16] . One of the greatest choices for supercapacitor systems is to use graphene as the electrode material due to its excellent electrical conductivity and large surface area[17-19]. Compared to batteries, it can charge and discharge rapidly and graphene can be employed for numerous charge-discharge cycles due to its extended cycle life[20]. Because of its high-power density, they are appropriate for portable devices and electric cars[21-23]. They are thought to hold promise for high-performance energy storage systems in the future [24, 25]. The discovery of graphene has proven that two-dimensional (2D) monolayer materials can be stable in the environment [26-28]. Their unique honeycomb structure gives them remarkable physical, chemical, and mechanical properties, which has attracted the attention of many researchers[29-31]. By stacking graphene with these two-dimensional materials[32], the fundamental properties of graphene are preserved while effectively tuning the bandgap, paving the way for the emergence of a new generation for low-power electronic devices [33,

*Corresponding author email: ksam.razaq@uobasrah.edu.iq

ISSN: 1817-2695 (Print); 2411-524X (Online)
Online at: https://jou.jobrs.edu.iq

34]. Since its early beginnings in the field of mechanically exfoliated graphene[36 ,35], the graphene industry has undergone significant development. There are currently several methods for manufacturing graphene, each with its own advantages and problems[37, 38]. Graphene is manufactured using top-down techniques such as graphite addition, pyrolysis, graphene oxide reduction, electrochemical scraping, wave excitation, etc. [39, 40], as well as bottom-up applications such as chemical vapor deposition (CVD), cumulative growth on SiC, and others [42 ,41]. Among these methods, liquid phase exfoliation is considered as one of the reliable methods to obtained graphene especially for supercapacitor purposes .In the recent years, the development of flexible supercapacitor systems has become essential because these systems have employes in many applications including wearable electronics such as smartwatches,[43] health-monitoring devices[44], flexible displays, electronic textiles, and portable biomedical sensors[45]. Therefore G is considered a highly promising material for flexible supercapacitors due to its excellent electrical conductivity, high surface area, and outstanding mechanical flexibility[46].

In this study the graphene was sandwich it in supercapacitor form after deposited it on Al thin sheet. The obtained assembly was used to develop the current working element to manufacture coil form (i.e large area graphene based flexible supercapacitor). All electrochemical measurements were carried out to ensure the suitability of the material in the case of a small surface area and/or in a large area SC.

Graphene is considered one of the distinguished materials for supercapacitors, but manufacturing these materials in large areas always faces problems and difficulties. Therefore, despite the crucial need for it in many applications, it is hard for the researchers to fabricate the electrodes in small areas, then developed the work into a large-scale form after confirming their high flexibility. This is essential and it lies in finding an effective method for designing and preparing electrodes with a good structure that allows for an increase in energy and power density, while maintaining electrode stability and a long operational life. The obtained device would be effective, large scale, flexible, and scalable. This is to direct efforts towards how to contribute to the development of these systems in the future.

2.Experimental details

2.1. Materials

Pure graphite powder, ethanol (with a purity of 99.99%), and sulphatic acid (with a purity of 99.99%) were purchased from a Sigma-Aldrich (Shanghai). All the chemicals were used as received without any additional treatments.

2.2. Synthesis of single/few layers of graphene

Using the LPE method and following the procedures described in the previous references [47, 48], single-layer or multi-layer graphene flakes in the nanometre range were obtained. Herein, 160 mg of graphite powder was added to a 400 ml glass beaker filled with 80 ml of 2-isopropanol (ISP). The beaker was then placed on a magnetic stirrer fitted with a heating plate for 60 minutes, until the graphite powder had completely dissolved and a homogeneous mixture was obtained. This mixture was transferred to an ultrasonicator, and to prevent excessive temperature rise during the exfoliation process, the glass beaker was immersed in an ice bath. An energy output ranging from 500 to 700 W was applied for 24 hours. Finally, the exfoliation process was successfully completed. During these stages, fresh ice was continuously replaced in the ice bath to maintain cooling throughout the exfoliation period using the LPE method. Fig. 1 shows a graphical representation of the synthesis process.

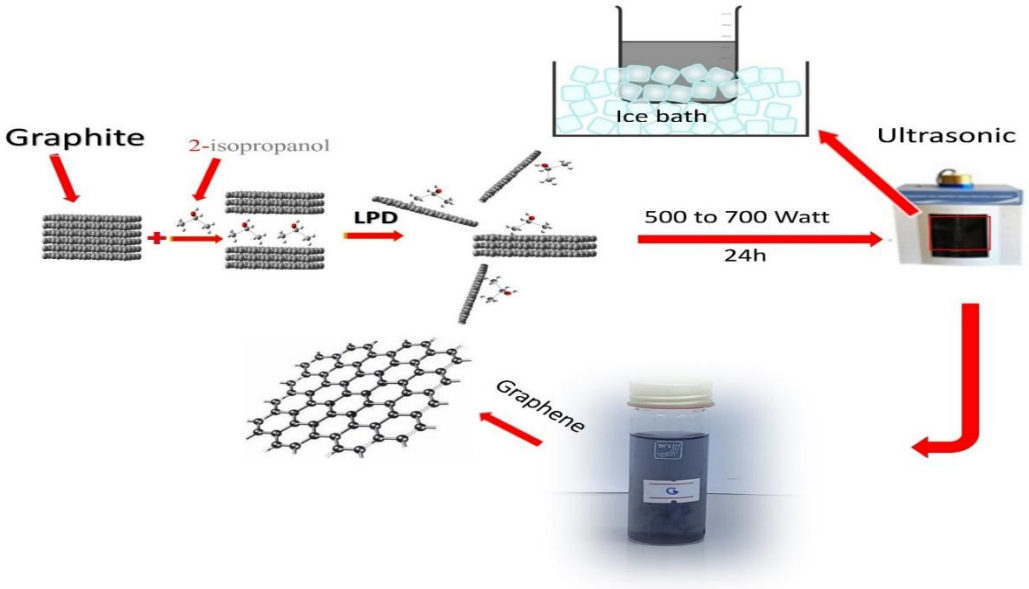

Fig. 1. Schematic illustration of the synthesis process of graphene

2.3. Electrode fabrication

The graphene was produced using a variety of equipment, including a vacuum drying oven (DZF-6020 from Tefic Blotech Ltd), a high-speed centrifuge (fitted with a cooling system) and an ultrasonic mixer (TF-1000 N from Tefic Blotech Ltd), and a magnetic heating plate equipped with an incubator and mixer (Joanlab, HPMS). A STEM system was used to examine the morphology of the materials obtained in this study. A PalmSens4 voltage/current measuring device (PalmSens, Netherlands), equipped with PStrace 5 software (version: 5.7), was used to study the electrochemical acitivies of the fabricated electrodes. The electrochemical tests included cyclic voltammetry (CV), device stability (charging and discharging), and EIS measurements. A locally fabricated test cell was connected to the PalmSens4 to accommodate the samples during the electrochemical measurements. The graphene mixture was deposited onto aluminum foil by drop-casting onto a preheated hotplate. Two pieces of identical size (3 × 1.5 cm²) were placed one on top of the other, separated by filter paper. A 0.2 M H_2SO_4 solution, as the electrolyte liquid, was then used to complete the supercapacitor assembly prior to the testing operating. A double test cell was used to house the assembled device and was connected to the PalmSens4 (PS) software to determine the electrochemical activity. The design of SC is shown in Fig. 2.

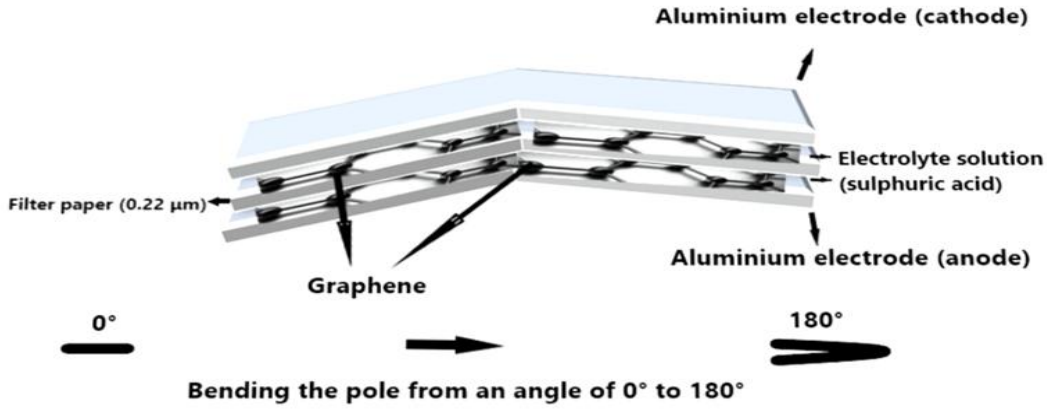

Fig. 2. The structure of the flexible supercapacitor device

3.Result and discussion

3.1. Structural analysis and surface morphology

Fig. 3 shows the X-ray diffraction (XRD) pattern of graphene, measured in the range of 2θ =10 to 90 degrees. A broad diffraction peak is observed, centred at approximately 26.4 degrees, which corresponds to (002) crystal plane of graphite. The broadness of this peak indicates that graphene consists of a few layers, and that the bonding strength between its layers is weaker than that found in bulk graphite. The faint broad peak appearing at approximately 43–45° is attributed to the (100)/(101) crystal plane of graphene. Overall, this XRD pattern (ICDD 41-1487) confirms that graphene consists of a few layers and that the stacking is partially disordered.

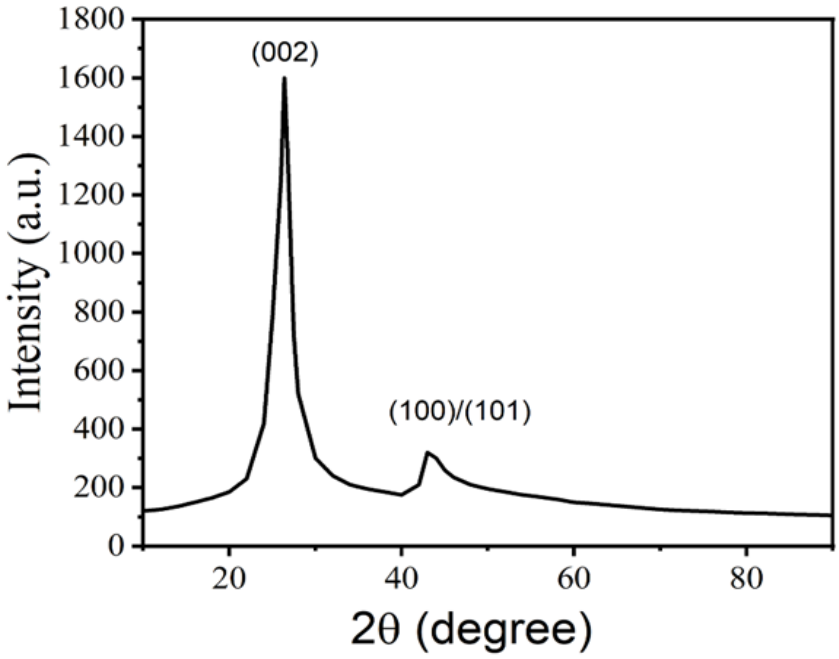

Fig.3. XRD pattern of graphene showing the characteristic (002) and (100)/ (101) diffraction planes.

The the scanning electron microscopy (STEM) images (see Fig. 4a–c) show several single- and multi-layer graphene flakes with transparent and wavy structures. The distinct differences in contrast in the images indicate regions of single-layer graphene, as well as regions where several layers of graphene are stacked on top of one another. The thin, plate-like structures with sharp edges confirm the successful exfoliation of graphite into graphene. In some areas, overlapping graphene layers were observed, which may have been related to repeated layer accumulation during the sample preparation or drying process. Overall, STEM results indicate the formation of high-quality single- and multi-layer graphene with minimal agglomeration. The dimensions of the observed flakes are approximately 200–400 nanometers. Overall, the image confirms the successful exfoliation of graphene nanoplates with nanoscale dimensions and a multi-layer morphology.

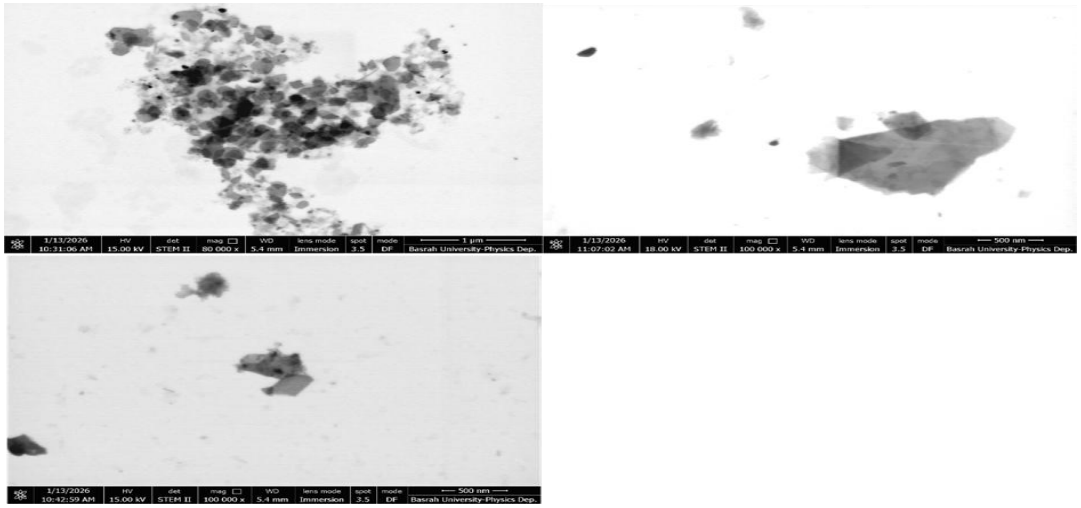

Fig. 4. (a-c) STEM results showing layers of graphene

3.2. Synthesis of small-scale graphene @ Al for supercapacitor

Two identical pieces of Graphene @Al (1.5 × 3 cm^2) were placed against each other in a sandwich form, with a liquid electrolyte of 0.2M H_2SO_4 above the porous filter, completing the flexible supercapacitor (FSC) structure. Fig 5a shows the real images of the prepared device. The flexible supercapacitor was conducted to a Plamsens4 device to measure its electrochemical properties under mechanical deformation. In our study, the bending state were examined in different angles. The electrochemical performance of the flexible supercapacitor was analyzed using cyclic voltammetry (CV) and other measurements. The electrochemical performance measurement results were obtained under various conditions, including the flat position (0° angle) and the curved position (up to 180° angle). The electrochemical performance measurement results are shown in Fig. 5 (b-h). The flexible cell consisting of a G@Al electrode was measured at different scan rates from 2 V/s to 0.05 V/s. In addition, inverted curves for G@Al are shown, which are explained by the oxidative and reductive activity resulting from reduction and oxidation processes[47-49]. All CV curves exhibit a nearly identical shape in different scan rates. The retention of the CV profiles under various mechanical deformation angles confirms the excellent flexibility and structural integrity of the electrode at different scan rates. It is encouraging that the voltage-current curve maintains its similar shape, indicating the device's excellent performance at this rate. The contribution of both capacitive and diffusion-controlled behaviour was illustrated. The cyclic voltammetry (CV) curve in 0.2 M H_2SO_4 also showed a larger enclosed area, reflecting enhanced capacitance due to improved proton conductivity and redox contributions[50]. Additional cyclic voltammetry (CV) and galvanostatic charge-discharge (GCD) analyses in the acidic electrolyte confirmed the persistence of pseudocapacitive behaviour even at higher scan rates.

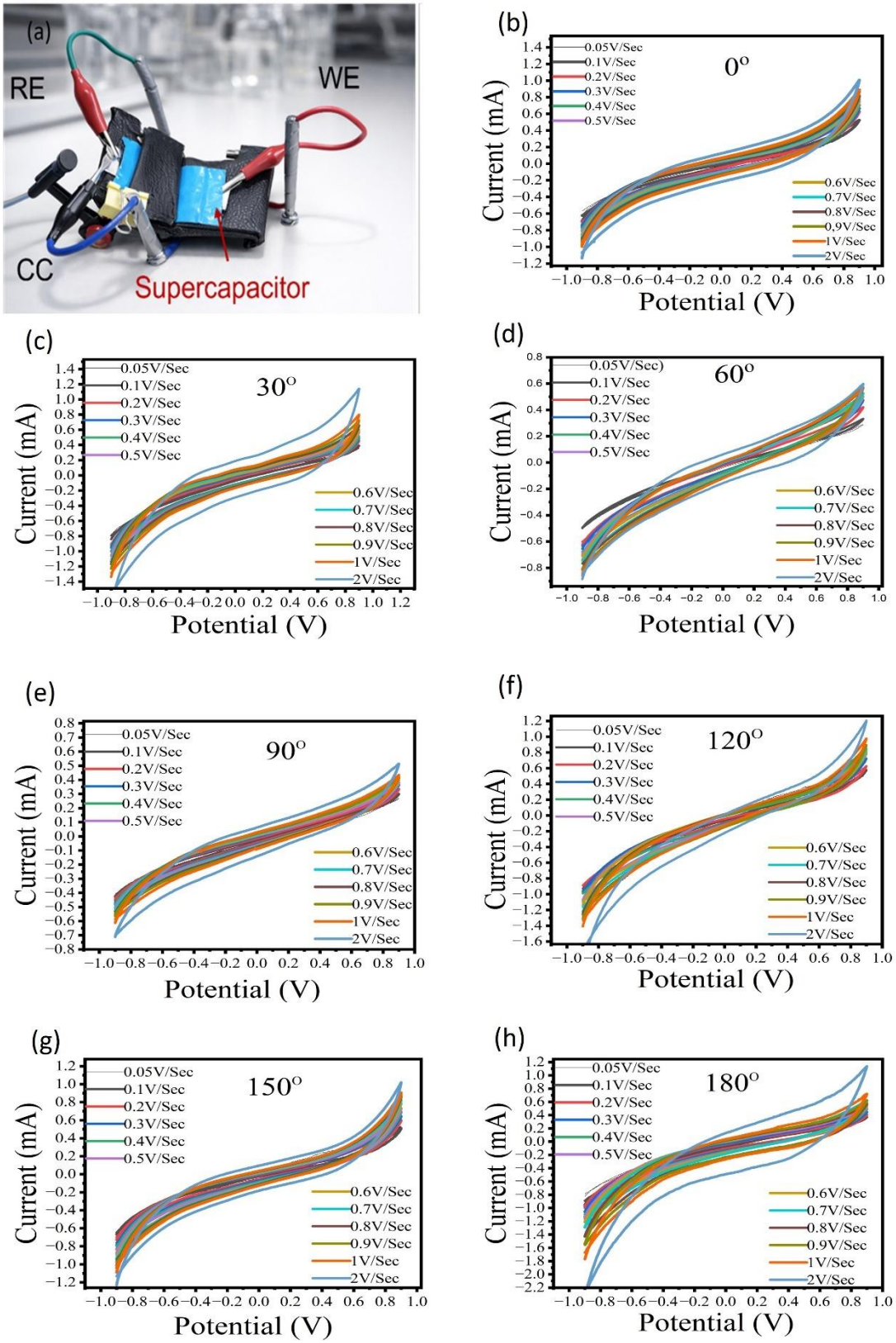

Fig. 5. (a) Photographic images of the locally manufactured flexible supercapacitor, (b-h) Electrochemical measurements of G@Al at different scan rates ranging from 0.05 V/s to 2V/s at bending angles of (0°, 30°, 60°, 90°, 120°, 150° and 180°), respectively.

The specific capacitance (C_{sp}) was calculated based on the cyclic voltage and current curves for each bending angle using the following formula [49].

$$C_{sp}=\frac{2\int I\,dV}{sm\Delta V} \quad (1)$$

Where m represents the mass of the two electrodes, ∫I dV represents the total area inside the voltage-current curve, I is the intensity of the current produced, s is the scan rate, and ΔV is the voltage window. The voltage window for the electrolyte (based on H_2SO_4) used in the work is 1.8V, and the C_{sp} values for all bending angles subject to mechanical deformation. All CV results are shown in Fig. 6.

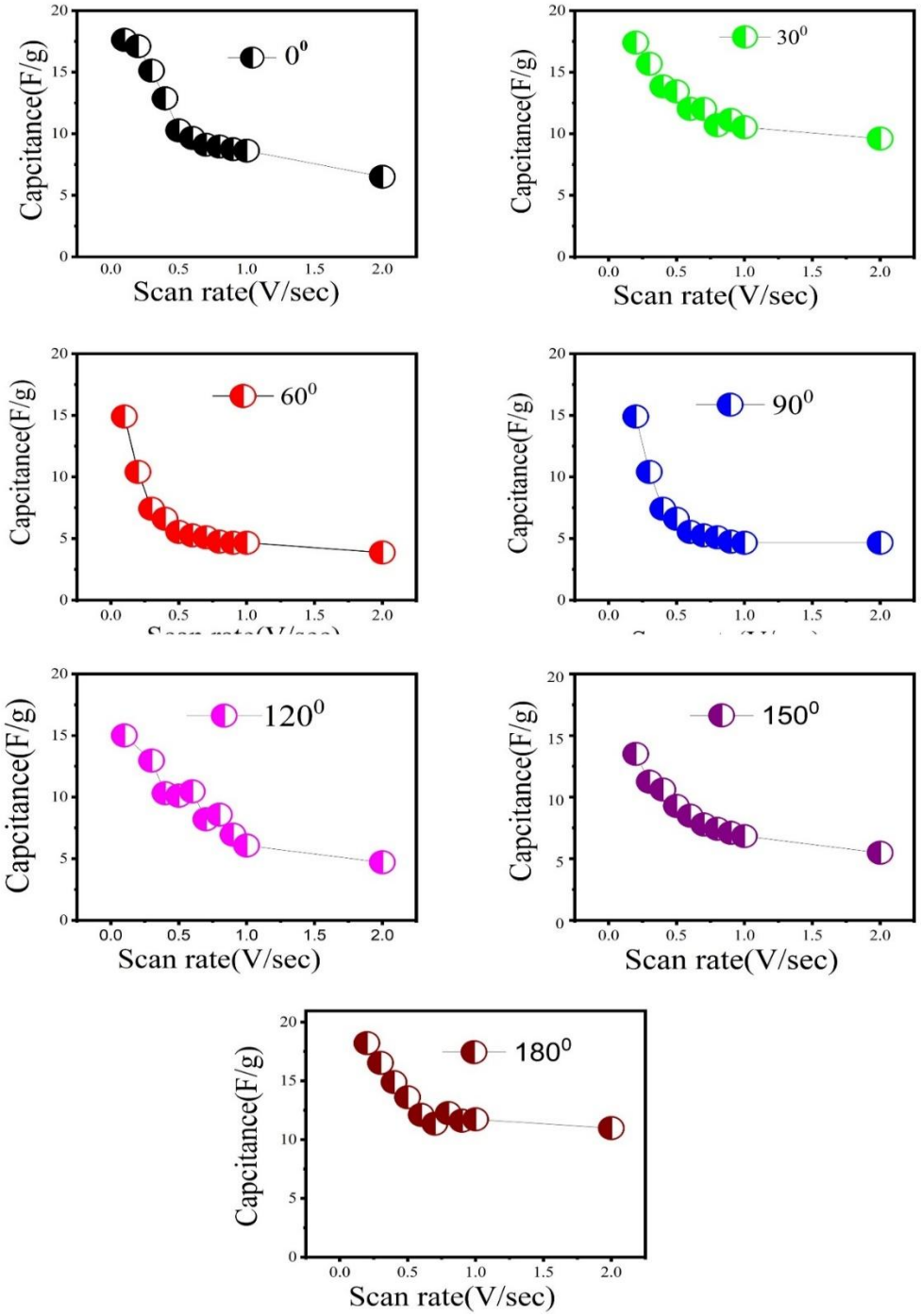

Fig.6. shows the specific capacitance of G@Al electrodes at different scanning rates and bending angles of 0°, 30°, 60°, 90°, 120°, 150°, and 180° using 0. 2M H_2SO_4 electrolyte.

Using a scanning speed of 1V/s, the C_{sp} are found to be 17.629, 17.395, 15.996, 14.902, 14.996,13.508 and 15.958 Fg^{-1}, in different bending conditions of 0 degrees, 30 degrees, 60 degrees, 90 degrees, 120 degrees, 150 degrees, and 180 degrees, respectively. This can be explained by the obstacle that the ions in the electrolyte fluids were able to overcome during bending, and by presenting the results in Fig. 6. This can be considered higher performance for the cell, whose electrode consists of G@Al due to the mechanical deformations it underwent, indicating that G@Al has flexible properties and suffered only minor damage under different bending conditions.

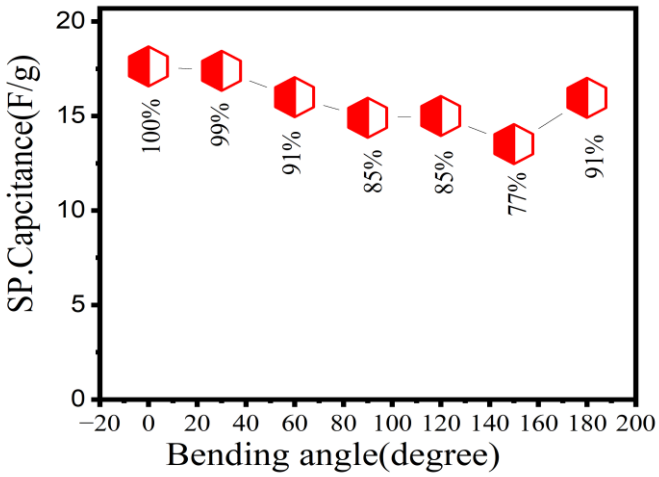

Fig. 7. C_{sp} versus bending angle for supercapacitors with bending angles of 0°, 30°, 60°, 90°, 120°, 150° and 180° at a fixed scan rate of 1V/s.

Fig. 8 shows CV curves for different bending angles at the same sweep rate (1 V/s). As can be seen, the CV curves are practically identical in all cases, and there are no additional peaks in the CV measurements after bending, which means that there is no interaction or change in the device.

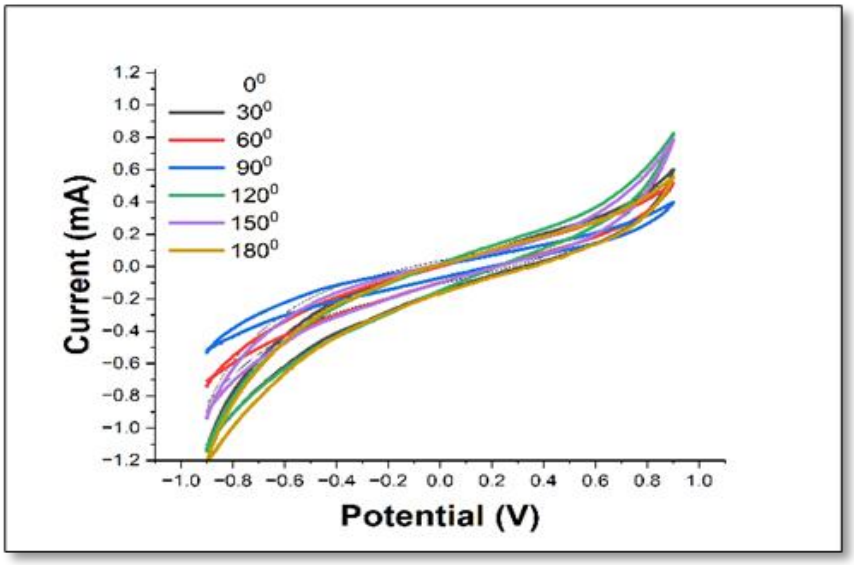

Fig.8. CV curves ata constant scanning speed of 1 V/sec for all angles of curvature.

Spectral measurements of electrochemical resistance (Nyquist plot) constitute an additional step to obtain more information on the capacitance behavior of G@Al. To do this, the measured data was fed into an equivalent circuit as shown in Fig.9 (using the free EIS Spectrum Analyzer software). The equivalent circuit consists of a series resistance of R1 resulting from contact and two RC elements,

(1C2) (R to match the low and high frequency regions). The second RC element is (CCPE R3 (where R3 represents the redox reaction resistance, R2 represents the charge transfer resistance, and CPE is a constant phase element representing the imaginary capacitance of the structure, which is an incomplete capacitance[51]. The equivalent circuit consists of a series resistance R_1 formed by the contact side and the RC circuit elements. (R_2C_1) to be proportional to the high and low frequency. The second RC is (R_3 CPE) where R_2 represents the resistance of oxidation-reduction reactions, R_3 represents the charge transfer resistance, and CPE (constant phase element) is considered the non-ideal capacitance, and it is the pseudo-capacitance part. The results of the circuit elements were collected from the composition of the equivalent circuit as in fig. 9a with the experimental data for the different bending angles (0°, 30°, 60°, 90°, 120°, 150°, and 180°) respectively, as shown in Table 1, where the results showed that the series resistance R_1 is between (3.401-16.832) Ω and the resistance R_2 is between 1454.4-1551.6 Ω, thus agreeing with the values for the real part of the measured impedance data at low frequency. To clarify the impedance results as indicated in fig 9(b-h), the CPE capacitance associated with G@Al values remained almost constant with the change of different bending angles (0°, 30°, 60°, 90°, 120°, 150°, and 180°) where their values are (34 ,35.8 ,34.4 ,29,32 ,36 ,33) μF, respectively. These further confirm the flexibility of G@Al.

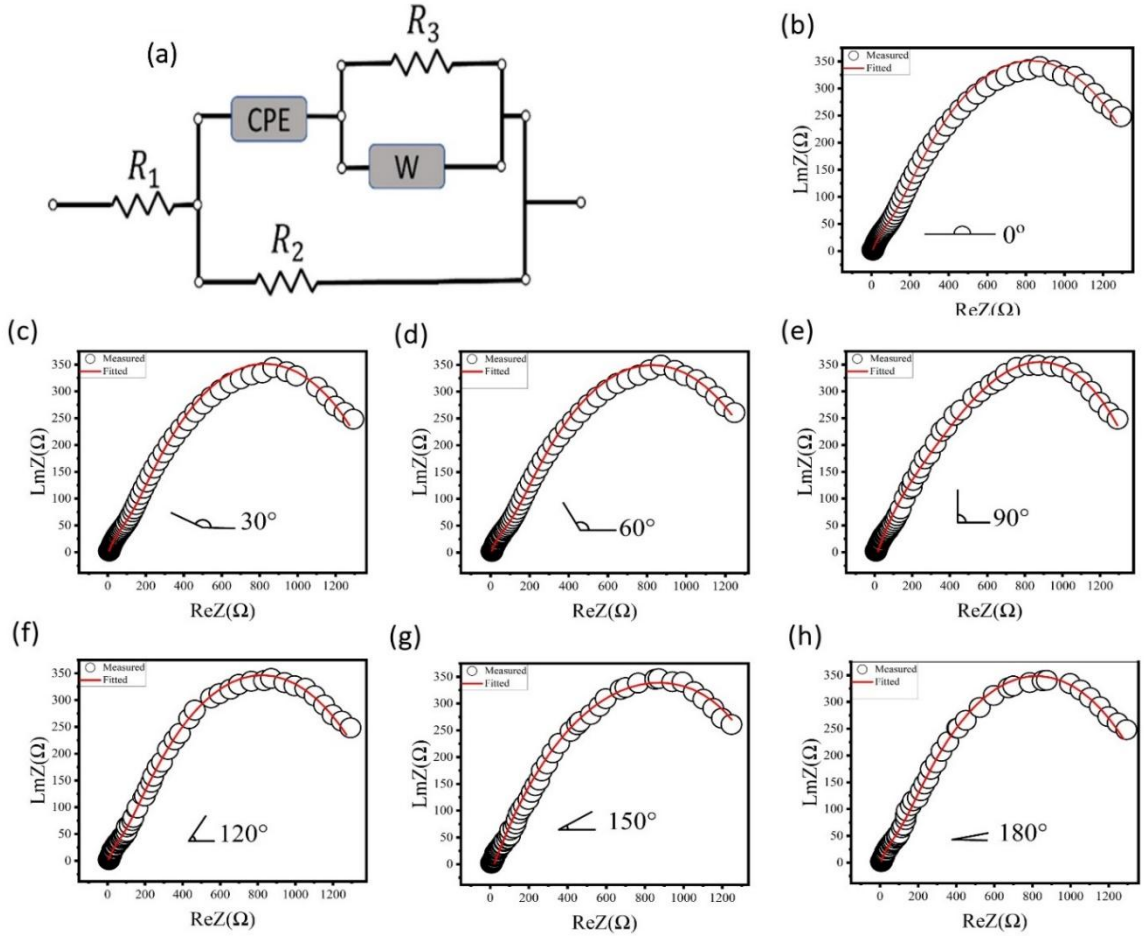

Fig. 9. (a) The equivalent circuits (b-h) Nyquist plot for electrochemical impedance spectroscopy (EIS) analysis in all bending angles from 0 to 180 degree.

All values of the equivalent circuit elements are derived from the proposed equivalent circuit for CPE, it is calculated based on the following equating

$$C_{CPE}=\frac{P}{[\omega^{1-n}\sin(\frac{n\pi}{2})]} \quad (2)$$

where ω is the angular frequency associated with the imaginary part, and P and n are structure coefficients.

Table 1. EIS parameters of the fabricated electrode

angle	$R_1(\Omega)$	$R_2(\Omega)$	$R_3(\Omega)$	W	P	n	CPE(μF)
0	4.529	1546.2	115.93	5286.1	0.0001869	0.57632	34
30	4.519	1546.3	116.6	5323.5	0.00018605	0.57727	35.8
60	3.8064	1551.6	108.61	5579.9	0.00018879	0.57067	34.4
90	16.832	1499.9	453.87	3148.1	0.00017551	0.57152	29
120	3.4485	1558.3	91.201	5349.5	0.00018851	0.55906	32
150	21.138	1454.4	6344.2	3296.1	0.00023784	0.58930	36
180	3.401	1549.9	102.75	5227.2	0.00018194	0.5677	33

The stability of the ultra-flexible cell, made from graphene and used in electrodes, was measured by subjecting it to 1000 charge-discharge cycles. As a result, it was found that the cell retained 93.5% of its initial capacity at 0° right up to the final cycle. To confirm this, Fig. 10a illustrates the stability of the flexible cell at 0°. Fig.10 (b-g) illustrates the stability of the flexible cell under bending angles of 30°, 60°, 90°,120°, 150°, 180° conditions. The flexible cell demonstrates good stability where C_{sp} retains 91% of its initial value at full bending, and 89.9% of its initial value after 1000 charge-discharge cycles after bending.

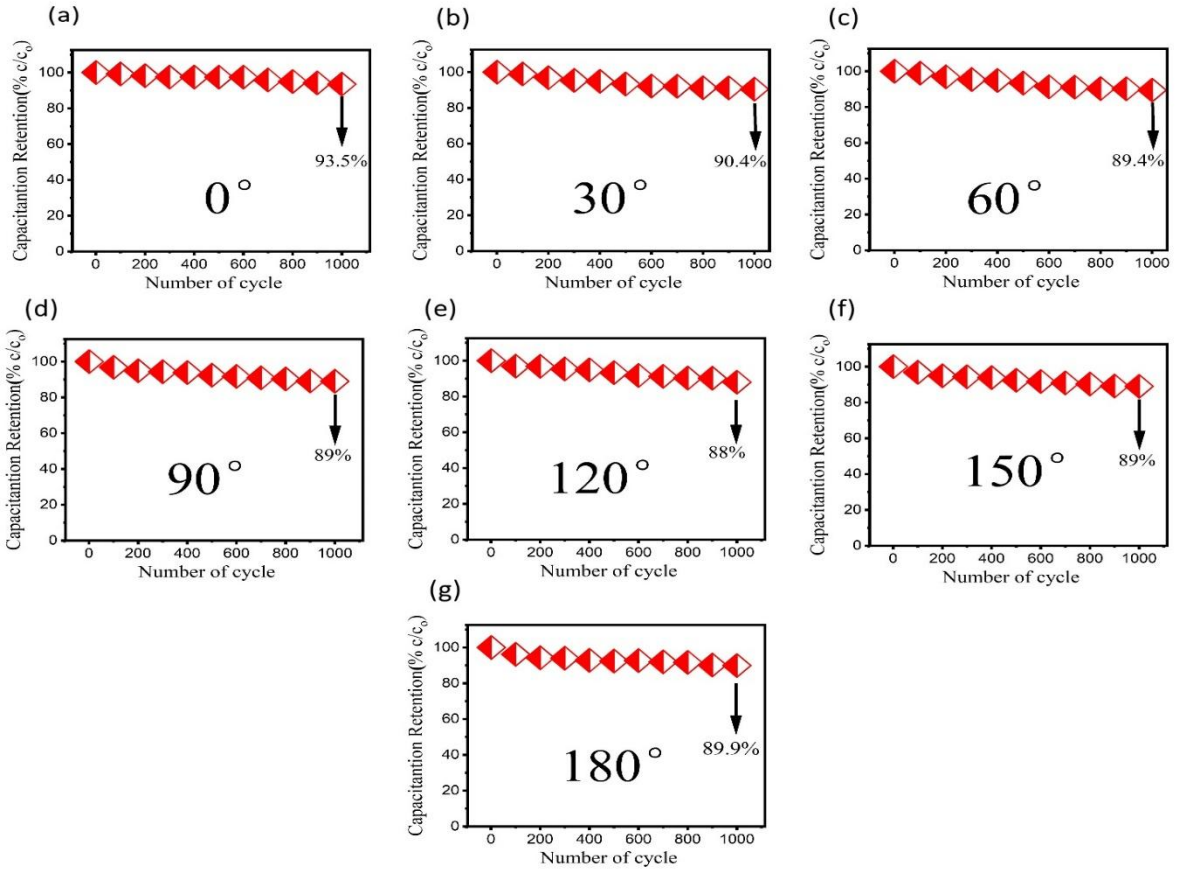

Fig. 10. shows the stability of the device capacity after 1000 cycles in all bending angles from 0 to 180 degree

The Ragone plot shows a comparison between the power and energy densities of the manufactured electrode sample GAl-LDH in graphical form. To calculate the amount of energy density in units (Wh/Kg) and the amount of power density in Watts/Kg, equations 3 and 4 are used [49] .

$$\text{Energy density (ED)} = \frac{CV^2}{2\,m'} \tag{3}$$

$$\text{Power density (PD)} = \frac{IV}{m'} \tag{4}$$

Where C represents the capacity obtained from the charge/discharge cycle, m′ is the mass of the electrode (without Al substrate), V is the voltage window, and I is the charge/discharge current. By calculating the energy density power density, it is found that the highest value of energy density for the flexible cell is 5.5 Wh/kg, while the highest value of energy density for the flexible cell is 5.73 kW/kg. As shown in Fig. 11, the high values for both may indicate the efficiency of the electrolyte, which contains an abundance of ions.

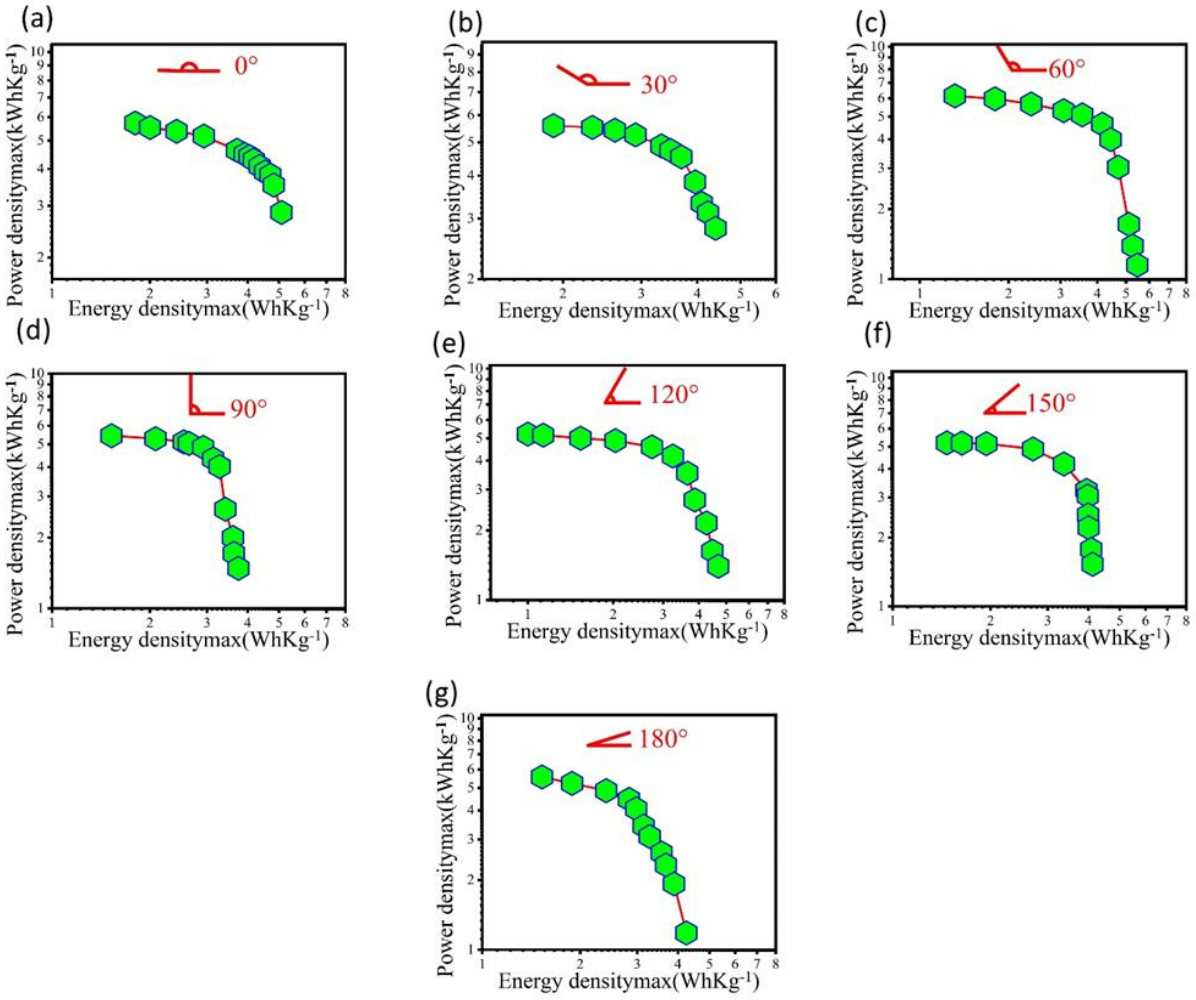

Fig. 11. (a-g) Illustrates the maximum ED and PD values for G@Al, in all bending angles from 0 to 180 degree

3.3. The development of graphene @ Al into large scale supercapacitor

To check the possibility of obtaining large scale SC, the prepared G@Al electrode was used as electrode using the benefits of flexibility confirmed in the last sections. In Fig.12, the electrochemical performance of the flexible cell consisting of a G@Al electrode was measured at a scan rate of 2 V/s to 0.05 V/s with an increase in electrode area (6×15 cm^2) and rolling the device creating the same two-electrode structure. The result is inverted curves for G@Al, which explain the oxidation and reduction activity resulting from reduction and oxidation processes. All CV curves have an almost identical shape at different scanning speeds. An increase in current of about 10 mA was observed, while maintaining the CV characteristics after cylindrical folding and preserving the integrity of the electrode structure. An increase in the specific capacity of the electrode was observed, reaching 123,774 Fg^{-1} compared to the previous state, where the highest specific capacity was 17,629 Fg^{-1}. As shown in Fig .12, the image shows the electrode before and after cylindrical folding.

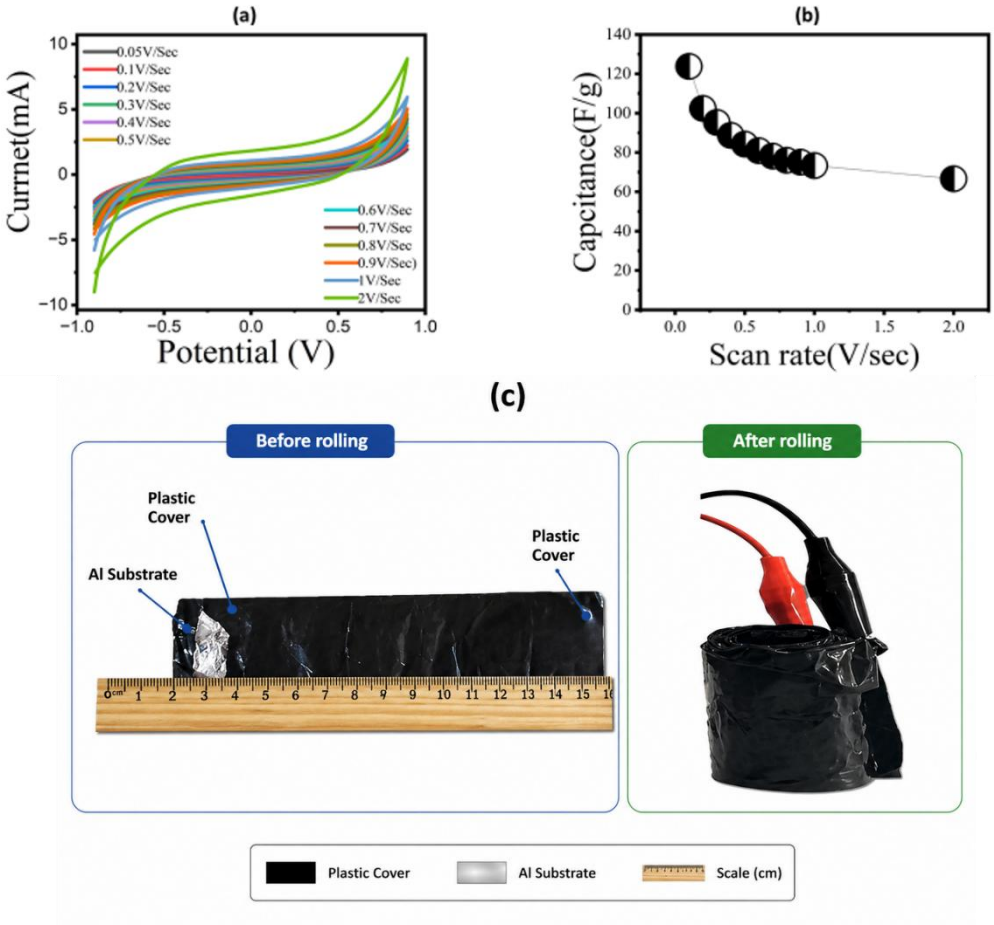

Fig. 12. Electrochemical performance of large area graphene based flexible supercapacitor based on G@Al. (a) shows the specific capacitance of the G@Al electrode at different scan rates, (b) shows the plot of the specific capacitance as a function of scan rate ranging from 0.05 V/s to 2 V/s after increasing the electrode area, (c) Images of the locally manufactured flexible supercapacitor and electrochemical measurements of G@Al.

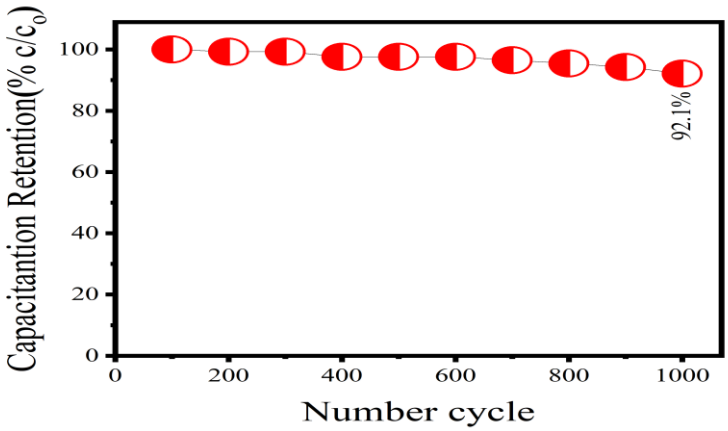

Fig. 13. The electrical capacitance of the device was found to remain stable after 1,000 cycles for the large-area graphene-based G@Al flexible supercapacitor

Fig 13 shows the stability of the highly flexible G@Al cells was evaluated by performing 1000 charge/discharge cycles. These cycles were repeated several times to verify the quality and stability of the cell. The results were compared with the initial capacity to assess the material's stability. The cell retains 92.1% of its initial capacity, confirming the good stability of the prepared electrodes even after prepared it in large scale.

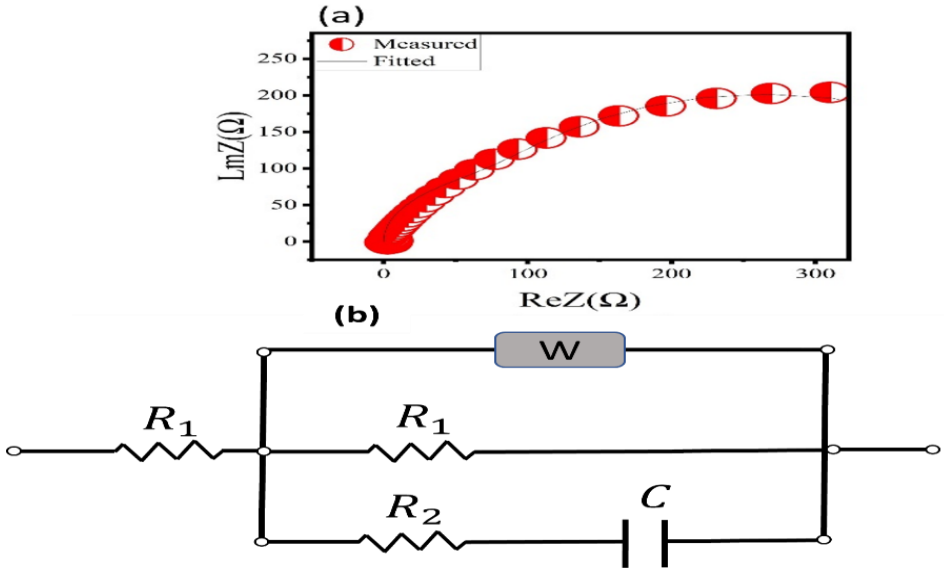

Fig.14. (a) EIS analysis for the Large area graphene based flexible supercapacitor (b) The equivalent circuits of the rolling device.

In Fig. 14, EIS analysis represents a further step towards obtaining more comprehensive information about the capacitive behaviour of G@Al over a wide range. For this purpose, the measurement data were plotted on an alternative graph, as shown in the figure, using the free software 'EIS Spectrum Analyzer'. The equivalent circuit consists of a series resistance R1, resulting from the junction, using the free EIS analysis software for each bending condition. The Nyquist plots are shown in Figure 14. The equivalent circuit (EC) contains a series resistance (R1 = 467.21 Ω), formed at the contact point, whilst in the high-frequency range, the second component is (CW), where (R2 = 268.14 Ω) represents the oxidation-reduction reaction resistance, W represents the diffusion resistance, and C represents a constant term

reflecting the capacitance of the structure. It was observed that the capacitance is 315 µF. Following the use of a large-area graphene-based flexible supercapacitor.

Table 2. EIS parameters of the fabricated electrode using the Large area graphene based flexible supercapacitor

Electrode	C(µF)	$R_1(\Omega)$	$R_2(\Omega)$	W
Al@G	315.3	467.21	268.14	10^7

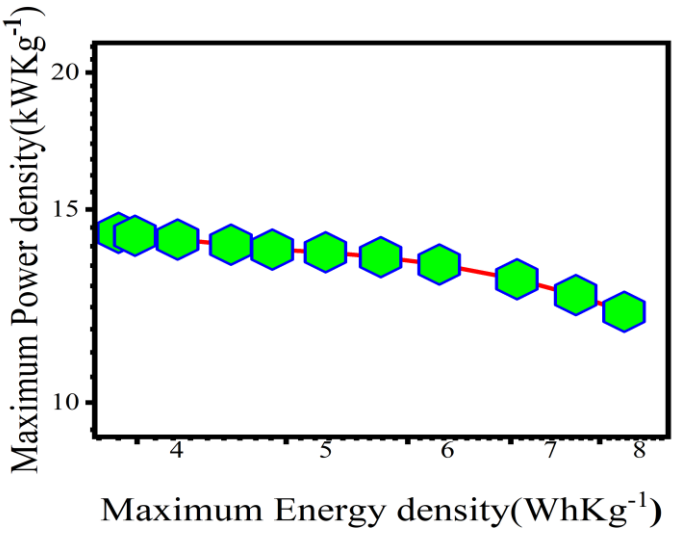

Fig. 15. Illustrates the maximum ED and PD values for G@Al Large area graphene based flexible supercapacitor

In the large-area supercapacitor fabricated using the wide-area flexible supercapacitor electrodes prepared as described in the previous sections, Equations (3) and (4) are used to calculate the energy density in W/kg and the capacitance density in W/kg. By calculating the power density and capacitance density, as shown in Fig .15, high values for both may indicate the efficiency of the electrolyte, which contains an abundance of ions and an increase compared to what was studied in previous research, following an increase in electrode area and the use of a large-area capacitor. The highest energy density value for the flexible cell was 8.1 W/kg, whilst the highest energy density value for the flexible cell was 14.3 kW/kg. This may indicate the efficiency of the electrolyte, which contains a high concentration of ions.

Table3 presents a comparison between the Csp, ED and PD values determined in this experiment and those previously published. The Csp value of the graphene-based supercapacitor, which is flexible and has a large surface area, is 8.86 times that of the MWCNT-COOH composite. It is three times greater than that of MWCNT and 1.9 times greater than that of pure MWCNT. The Csp values under all bending conditions remain similar to those of the other materials listed in Table 2. This test demonstrated high energy density, which is consistent with other reports. The specific energy reached 14.3 kW/kg, which is 1.27 times greater than that of RuO_2/MWCNT. Bending affects PD, but in the case of rotation, an approximately constant value was obtained due to the geometric parameters of the electrodes. In general, ED is higher than that found in most devices mentioned in the reports and depends on the type of electrolyte solution. The highest ED and PD values recorded in our reports were compared with data from previous studies, as shown in Table 3. All devices fabricated using H_2SO_4 as the electrolyte exhibited good electrochemical parameters, particularly high PD values.

Table 3. presents a comparison between the Cspc, ED and PD values

Electrode material Ref	Electrolyte	Max Csp (F/g)	PD (kW/kg)	ED (W h/kg)
MnO2/carbon nanotube [52]	0.1 M Na_2SO_4	44	11	2.9
RuO2/MWCNT [53]	1MH_2SO_4	147	0.5	36.8
PristineMWCNTs [54]	6MKOH	16.6	…	0.58
MWCNT-COOH [54]	1MKOH	8.5	…	0.29.
MWCNT [55]	6MKOH	16	N/A	N/A
In_2O_3 NWs/carbon nanotube [56]	Non-aqueous	64	7.48	1.29
G/Al -0º This Work	0.2M H_2SO_4	17.629	5.73	5
G/Al-30º This Work	0.2M H_2SO_4	17.395	5.6	4.4
G/Al -60º This Work	0.2M H_2SO_4	15.996	6.14	5.5
G/Al -90º This Work	0.2M H_2SO_4	14.902	5.4	3.7
G/Al -120º This Work	0.2M H_2SO_4	14.996	5.2	4.7
G/Al -150º This Work	0.2M H_2SO_4	13.508	5.2	4.1
G/Al -180º This Work	0.2M H_2SO_4	15.958	5.7	4.3
G/Al large area This Work	0.2M H_2SO_4	123.774	14.3	8

4.Conclusion

The results of this work include the fabrication of G@Al electrodes using LPE technology for a flexible supercapacitor after bending at various angles ranging from 0° to 180°. The use of simple and well-known chemical preparation techniques, which rely on a single-step reaction process to synthesize graphene on a flexible aluminum substrate, is considered. Electronic studies (such as STEM and X-ray) showed consistent results in terms of obtained graphene sheets with few/single layers with high crystallin structure. Excellent results were obtained in terms of high stability, large storage capacity, and high energy density, despite the mechanical deformation resulting from bending the supercapacitor at various angles (0°, 30°, 60°, 90°, 120°, 150° and 180°, respectively). The strong mechanical properties and unique shape are attributed to the formation of G-layers on the surface of the aluminum foils, which resulted a large effective area. The CV curve reflectivity operates within a voltage range of -0.9 to 0.9 V obtained maximum specific capacitance of 17.629 Fg^{-1} in the flat state and a close value of 16 Fg^{-1} at 180 degrees. It also delivered high ED of 5.5 W/kg and PD of 5.73 kW/kg. The supercapacitors also have a long service life and retain at least 93.5% of their capacity after 1000 charge/discharge cycles. The decrease in electrochemical performance may be related to the sensitivity of the electrodes to moisture after bending, as there are no changes in the morphology of the electrode materials.

The equivalent circuit of the model was obtained by plotting a Nyquist plot to analyse the EIS. By using a large-area flexible graphene-based supercapacitor, the results of our study improved, with a measured specific capacitance of 123.774 F/g observed in this case. Furthermore, it was observed that the cell retained 92.1% of its initial capacity after 1,000 charge/discharge cycles, indicating electrode stability; similarly, upon implementation, the equivalent circuit of the model was obtained by plotting

a Nyquist plot for EIS analysis. A high energy density of 8.1 W/kg and a power density of 14.3 kW/kg were achieved following the process.

References

[1] H. Wang, T. Liu, H. Xu, E. Dai, and H. Hou, "Synergy of carbon-pollution-ecology——The future of synergetic reduction of pollution and carbon emissions," *Environmental Impact Assessment Review*, vol. 114, p. 107931, 2025.

[2] A. Gu, F. Teng, and X. Feng" ,Effects of pollution control measures on carbon emission reduction in China: evidence from the 11th and 12th Five-Year Plans," *Climate Policy*, vol. 18, no. 2, pp. 198-209, 2018.

[3] Q. Xiao, Y. Zhao, S. Shen, Z. Zheng, and M. Zhao, "The impact of environmental tournament on CO2 emissions from the perspective of synergizing the reduction of pollution and carbon emissions," *Science of the Total Environment*, vol. 907, p. 168181, 2024.

[4] I. Akhtar, S. Kirmani, and M. Jameel, "Reliability assessment of power system considering the impact of renewable energy sources integration into grid with advanced intelligent strategies," *IEEE Access*, vol. 9, pp. 32485-32497, 2021.

[5] S. Kumar, R. Saket, D. K. Dheer, J. B. Holm-Nielsen, and P. Sanjeevikumar, "Reliability enhancement of electrical power system including impacts of renewable energy sources: a comprehensive review," *IET Generation, Transmission & Distribution*, vol. 14, no. 10, pp. 1799-1815, 2020.

[6] M. M. Islam *et al.*, "Improving reliability and stability of the power systems: A comprehensive review on the role of energy storage systems to enhance flexibility," *IEEE Access*, vol. 12, pp. 152738-152765, 2024.

[7] H. Li, Z. Tang, Z. Liu, and C. Zhi, "Evaluating flexibility and wearability of flexible energy storage devices," *Joule*, vol. 3, no. 3, pp. 613-619, 2019.

[8] L. Kong, C. Tang, H. J. Peng, J. Q. Huang, and Q. Zhang, "Advanced energy materials for flexible batteries in energy storage: A review," *SmartMat*, vol. 1, no. 1, 2020.

[9] S. A. Hammood, A .S. Al-Asadi, and M. F. Al-Mudhaffer, "Synthesis and properties of flexible supercapacitor based on zinc-aluminum layered doubled hydroxide," *Journal of Alloys and Compounds*, vol. 1009, p. 176925, 2024.

[10] S. Gupta, W. T. Navaraj, L. Lorenzelli, and R .Dahiya, "Ultra-thin chips for high-performance flexible electronics," *npj Flexible Electronics*, vol. 2, no. 1, p. 8, 2018.

[11] S. Garner, S. Glaesemann, and X. Li, "Ultra-slim flexible glass for roll-to-roll electronic device fabrication," *Applied Physics A*, vol. 116, no. 2, pp. 403-407, 2014.

[12] M. Zhu, F. Zhu, and O. G. Schmidt, "Nano energy for miniaturized systems," *Nano Materials Science*, vol. 3, no. 2, pp. 107-112, 2021.

[13] S. A. Hammood and A. S. Al-Asadi, "Flexible electrochemical supercapacitors: a review," *Basrah Journal of Science*, vol. 42, no. 1, pp. 23-51, 2024.

[14] W. Zhao, M. Jiang, W. Wang, S. Liu, W. Huang, and Q. Zhao, "Flexible transparent supercapacitors: materials and devices," *Advanced Functional Materials*, vol. 31, no. 11, p . .2021 ,2009136

[15] Q. Wu *et al.*, "Cyclic stability of supercapacitors: materials, energy storage mechanism, test methods, and device," *Journal of Materials Chemistry A*, vol. 9, no. 43, pp. 24094-24147, 2021.

[16] X. Wang, X. Lu, B. Liu, D. Chen, Y. Tong ,and G. Shen, "Flexible energy-storage devices: design consideration and recent progress," *Advanced materials*, vol. 26, no. 28, pp. 4763-4782, 2014.

[17] A. S. Lemine, M. M. Zagho, T. Altahtamouni, and N. Bensalah, "Graphene a promising electrode material for supercapacitors—A review," *International Journal of energy research,* vol. 42, no. 14, pp. 4284-4300, 2018.
[18] Z. S. Iro, C. Subramani, and S. Dash, "A brief review on electrode materials for supercapacitor," *International Journal of Electrochemical Science,* vol. 11, no. 12, pp. 10628-10643, 2016.
[19] R. Dubey and V. Guruviah, "Review of carbon-based electrode materials for supercapacitor energy storage," *Ionics,* vol. 25, no. 4, pp. 1419-1445, 2019.
[20] A. I. Habeeb and A. S. Al-Asadi, "Fabrication of hybrid graphene nanosheets/Vanadium (V) oxide nanoparticles composite electrodes for supercapacitor application," *Solid State Communications,* vol. 360, p. 115024, 2023.
[21] S. Rosenthal, F. Maaß, M. Kamaliev, M. Hahn, S. Gies, and A. E. Tekkaya, "Lightweight in automotive components by forming technology," *Automotive Innovation,* vol. 3, no. 3, pp. 195-209, 2020.
[22] B. H. Nguyen and V. H. Nguyen, "Promising applications of graphene and graphene-based nanostructures," *Advances in Natural Sciences: Nanoscience and Nanotechnology,* vol. 7, no. 2, p. 023002, 2016.
[23] M. Hepel, "Advances in micro-supercapacitors (MSCs) with high energy density and fast charge-discharge capabilities for flexible bioelectronic devices—A review," *Electrochemical Science Advances,* vol. 3, no. 3, p. e2100222, 2023.
[24] E. Pomerantseva, F. Bonaccorso, X. Feng, Y. Cui, and Y. Gogotsi, "Energy storage: The future enabled by nanomaterials," *Science,* vol. 366, no. 6468, p. eaan8285, 2019.
[25] A. Aghmadi and O. A. Mohammed, "Energy storage systems: technologies and high-power applications," *Batteries,* vol. 10, no. 4, p. 141, 2024.
[26] A. K. Geim and K. S. Novoselov, "The rise of graphene," *Nature materials,* vol. 6, no. 3, pp. 183-191, 2007.
[27] S. S. Varghese, S. H. Varghese ,S. Swaminathan, K. K. Singh, and V. Mittal, "Two-dimensional materials for sensing: graphene and beyond," *Electronics,* vol. 4, no. 3, pp. 651-687, 2015.
[28] D. Akinwande *et al.*, "Graphene and two-dimensional materials for silicon technology," *Nature,* vol. 573, no. 7775, pp. 507-518, 2019.
[29] L. T. Siow, J. R. Lee, E. H. Ooi, and E. Von Lau, "Application of graphene and graphene derivatives in cooling of photovoltaic (PV) solar panels: A review," *Renewable and Sustainable Energy Reviews,* vol. 193, p. 1.2024 ,14288
[30] J. Wu, H. Lin, D. J. Moss, K. P. Loh, and B. Jia, "Graphene oxide for photonics, electronics and optoelectronics," *Nature Reviews Chemistry,* vol. 7, no. 3, pp. 162-183, 2023.
[31] T. Han *et al.*, "Orbital multiferroicity in pentalayer rhombohedral graphene," *Nature,* vol. 623, no. 7985, pp. 41-47, 2023.
[32] M. A. Al-Hamyd, A. S. Al-Asadi, and M. F. Al-Mudhaffer, "Preparation and characterization of zinc–aluminum layered doubled hydroxide/graphene nanosheets composite for supercapacitor electrode," *Physica E: Low-dimensional Systems and Nanostructures,* vol. 136, p. 115005, 2022.
[33] P. Lu, W. Chen, J. Chen, X. Li, S. Li, and B. Bian, "Interfacial properties of ZrSX/Graphene (X= O, Se) heterostructures with the modulation of electric field and defect engineering," *Physica E: Low-dimensional Systems and Nanostructures,* p. 116436, 2025.
[34] K. Khan *et al.*, "Recent developments in emerging two-dimensional materials and their applications," *Journal of Materials Chemistry C,* vol. 8, no. 2, pp.2020 ,387-440 .
[35] Y. Sun *et al.*, "Mechanical properties of graphene," *Applied Physics Reviews,* vol. 8, no. 2, 2021.
[36] M. Yi and Z. Shen, "A review on mechanical exfoliation for the scalable production of graphene," *Journal of Materials Chemistry A* ,vol. 3, no. 22, pp. 11700-11715, 2015.

[37] Z. Liu, S. P. Lau, and F. Yan, "Functionalized graphene and other two-dimensional materials for photovoltaic devices: device design and processing," *Chemical Society Reviews,* vol. 44, no. 15, pp. 5638-5679, 2015.
[38] T. Palacios, A. Hsu, and H. Wang, "Applications of graphene devices in RF communications," *IEEE Communications Magazine,* vol. 48, no. 6, pp. 122-128, 2010.
[39] Y. Yan *et al.,* "Synthesis of graphene: Potential carbon precursors and approaches," *Nanotechnology Reviews,* vol. 9, no. 1, pp. 1284-1314, 2020.
[40] H. El Etri, "Graphene: A state-of-the-art review of types, properties and applications in different sectors," *Prabha Mater. Sci. Lett.,* vol. 2, no. 2, pp. 98-139, 2023.
[41] A. E. Kaloyeros and B. Arkles, "Silicon carbide thin film technologies: Recent advances in processing, properties, and applications: Part II. PVD and alternative (non-PVD and non-CVD) deposition techniques," *ECS Journal of Solid State Science and Technology,* vol. 13, no. 4 ,p. 043001, 2024.
[42] M. Sabzi *et al.,* "A review on sustainable manufacturing of ceramic-based thin films by chemical vapor deposition (CVD): reactions kinetics and the deposition mechanisms," *Coatings,* vol. 13, no. 1, p. 188, 2023.
[43] K. Keum, J. W. Kim, S. Y. Hong, J. G. Son, S. S. Lee, and J. S. Ha, "Flexible/stretchable supercapacitors with novel functionality for wearable electronics," *Advanced Materials,* vol. 32, no. 51, p. 2002180, 2020.
[44] G. Jung *et al.,* "Temperature-tolerant flexible supercapacitor integrated with a strain sensor using an organohydrogel for wearable electronics," *Chemical Engineering Journal,* vol. 450, p. 138379, 2022.
[45] M. G. Say *et al.,* "Scalable paper supercapacitors for printed wearable electronics," *ACS Applied Materials & Interfaces,* vol. 14, no. 50, pp. 55850-55863, 2022.
[46] S. Shalini, T. Naveen, D. Durgalakshmi, S. Balakumar, and R. A. Rakkesh, "Progress in flexible supercapacitors for wearable electronics using graphene-based organic frameworks," *Journal of Energy Storage,* vol. 86, p. 111260, 2024.
[47] A. Ciesielski and P. Samorì, "Graphene via sonication assisted liquid-phase exfoliation," *Chemical Society Reviews,* vol. 43, no. 1, pp. 381-398, 2014.
[48] W. K. Chee, H. N. Lim, Z. Zainal, N. M. Huang, I. Harrison, and Y. Andou, "Flexible graphene-based supercapacitors: a review," *The Journal of Physical Chemistry C,* vol. 120, no. 8, pp. 4153-4172, 2016.
[49] A. S. Al-Asadi *et al.,* "Fabrication and characterization of ultraviolet photosensors from ZnO nanowires prepared using chemical bath deposition method," *Journal of Applied Physics,* vol. 119, no. 8, 2016.
[50] V. Šedajová, P. Jakubec, A. Bakandritsos, V. Ranc, and M. Otyepka, "New limits for stability of supercapacitor electrode material based on graphene derivative," *Nanomaterials,* vol. 10, no. 9, p. 1731, 2020.
[51] N. Menachery, S. Thomas, B. Deepanraj, and N. Senthilkumar, "Processing of nanoreinforced aluminium hybrid metal matrix composites and the effect of post-heat treatment: a review," *Applied Nanoscience,* vol. 13, no. 6, pp. 4075-4099, 2023.
[52] A. L. M. Reddy, M. M. Shaijumon, S. R. Gowda, and P. M. Ajayan, "Multisegmented Au-MnO2/carbon nanotube hybrid coaxial arrays for high-power supercapacitor applications," *The Journal of Physical Chemistry C,* vol. 114, no. 1, pp. 658-663, 2010.
[53] A. L. M. Reddy and S. Ramaprabhu, "Nanocrystalline metal oxides dispersed multiwalled carbon nanotubes as supercapacitor electrodes," *The Journal of Physical Chemistry C,* vol. 111, no. 21, pp. 7727-7734, 200.7

[54] A.-R. Rautio *et al.*, "Electric double-layer capacitors based on multiwalled carbon nanotubes: can nanostructuring of the nanotubes enhance performance?," *The Journal of Physical Chemistry C*, vol. 119, no. 7, pp. 3538-3544, 2015.
[55] A. S. Al-Asadi *et al.*, "Aligned carbon nanotube/zinc oxide nanowire hybrids as high performance electrodes for supercapacitor applications," *Journal of Applied Physics*, vol. 121, no. 12, 2017.
[56] P.-C. Chen, G. Shen, S. Sukcharoenchoke, and C. Zhou, "Flexible and transparent supercapacitor based on In2O3 nanowire/carbon nanotube heterogeneous films," *Applied Physics Letters*, vol. 94, no. 4, 2009.

Journal of Basrah Researches (Sciences) **52**(1), 204 (2026)
DOI: https://doi.org/10.56714/bjrs.52.1.15

قطب كهربائي مرن من الجرافين لمكثف فائق مرن عالي الأداء؛ قطب كهربائي واسع المساحة قائم على الجرافين

قسام رزاق حسن الخفاجي*، أحمد صالح الاسدي

قسم الفيزياء, كلية التربية للعلوم الصرفة، جامعة البصرة.

معلومات البحث

الاستلام 23 شباط 2026
المراجعة 27 نيسان 2026
القبول 28 نيسان 2026
النشر 30 حزيران 2026

الكلمات المفتاحية

مكثفات فائقة، الغرافين، المرونة

Citation: Q. R. Hasan, A. S. Al-Asadi. , J. Basrah Res. (Sci.) **52**(1), 204 (2026). DOI:https://doi.org/10.56714/bjrs.52.1.15

الملخص

في هذا التقرير، تم تصنيع طبقات من الجرافين (G) على سطح ركيزة من الألومنيوم (Al) لتكوين قطب كهربائي لمكثف فائق .(SC) واستُخدمت مادة G@Alالناتجة كأقطاب كهربائية مرنة، وأظهرت استقرارًا جيدًا في قياس الجهد الدوري المتكرر إلى جانب كثافة طاقة وكثافة قدرة جيدتين. تبلغ السعة النوعية القصوى في الظروف المستوية حوالي17.629 F/g ، ولم تنخفض هذه القيمة بأكثر من 9.4% بعد ثني الجهاز بزوايا 30 و60 و90 و120 و150 و180 درجة. أظهر G@Al استقرارًا جيدًا، حيث استعاد 93.5% من قيمته الأولية بعد 1000 دورة .وقد وجد أن الحد الأقصى لـ ED وPD يصل إلى 5.5Wh/kg و kW/kg 5.73على التوالي، وأظهر EIS أداءً كهروكيميائيًا جيدًا، وأظهرت الدائرة المتدفقة أربعة مقاومات و CPE جنبًا إلى جنب مع عنصر .W تطوير SC الذي تم الحصول عليه من خلال إنشاء جهاز مكثف فائق مرن قائم على الجرافين ذي مساحة كبيرة والذي أظهر سعة محددة أعلى تبلغ 123.774 Fg^{-1} جنبًا إلى جنب مع مرونة فائقة.

***Corresponding author email:** ksam.razaq@uobasrah.edu.iq

ISSN: 1817-2695 (Print); 2411-524X (Online)
Online at: https://jou.jobrs.edu.iq